Director configurations of nematic-liquid-crystal droplets: Negative dielectric anisotropy and parallel surface anchoring

F. Xu, H.-S. Kitzerow, and P. P. Crooker
Department of Physics and Astronomy, University of Hawaii, Honolulu, Hawaii 96822
(Received 30 August 1993)

We have identified the director configurations $\mathbf{n}(\mathbf{r})$ of nematic droplets subjected to electric fields under conditions of negative dielectric anistropy and parallel surface anchoring. Drops are examined using polarization microscopy, with electric fields applied parallel or perpendicular to the light direction. The behavior of the resulting textures and defects is obtained by comparing the droplet appearance with computer simulated transmission patterns using intuitively obtained model director configurations. In the field-off state, the director is essentially azimuthal (concentric texture) near the surface, "escaping" to the axis direction (bipolar texture) along the droplet axis. For low fields, the director configuration becomes either more bipolar or more concentric depending on whether the droplet axis is initially parallel or perpendicular to the electric field. For high fields, the bipolar structure evolves into one in which the directors form planar bipolar sheets escaped at the poles (escaped planar bipolar texture). The concentric structure, however, becomes unstable and a novel transition to the more stable escaped planar bipolar structure is described.

PACS number(s): 61.30.Gd, 61.30.Jf

I. INTRODUCTION

When a nematic liquid crystal is confined between orienting boundaries, the competition between surface ordering and bulk elastic deformation can produce a variety of unusual director configurations [defined as $\mathbf{n}(\mathbf{r})$] [1]. These configurations, which depend on the elastic constant ratio and the orientation and strength of the boundary conditions, may also incorporate one or more defects, which appear either on the surface or in the bulk [2,3].

When, in addition, an electric field is applied, a further competition arises which causes the structures and defects to evolve in various ways according to the size and sign of the dielectric anisotropy [2–4]. The resulting director configurations and defect locations are difficult to predict analytically, especially for certain conditions. For *perpendicular* boundary conditions, a unique (perpendicular) director orientation is specified at the surface. This unique surface orientation allows one to make reasonable guesses at the bulk director orientation. For *parallel* boundary conditions with no specified direction, however, the preferred surface orientation is not unique. In this case the director can point in any direction on the boundary, and the resulting bulk structure is, unlike the case of perpendicular boundary conditions, much more difficult to guess.

Likewise, for *positive* dielectric anisotropy, the electric field direction and preferred bulk director orientation are the same. One can therefore anticipate the resulting texture. For *negative* dielectric anisotropy, however, the field specifies the *nonpreferred* orientation, thereby leaving the director's remaining two degrees of freedom unspecified, ultimately to be determined by the system itself. For such systems it is much more difficult to anticipate the final texture.

The director configurations of liquid crystals confined to spherical droplets have recently been much investigated, both for their scientific interest [5] and as a result of their use in practical displays [1]. For strong anchoring conditions, (no deviation from the surface-preferred directions), the director configuration can be determined, at least in principle, by minimizing the free energy,

$$F=\tfrac{1}{2}\int [k_1(\nabla\cdot\mathbf{n})^2+k_2(\mathbf{n}\cdot\nabla\times\mathbf{n})^2 +k_3(\mathbf{n}\times\nabla\times\mathbf{n})^2-\epsilon_0\epsilon_a(\mathbf{E}\cdot\mathbf{n})^2]dV\ . \quad (1)$$

Here $\mathbf{n}$ is the director k_1, k_2, k_3 are elastic constants, ϵ_a is the dielectric anisotropy ($\epsilon_\parallel-\epsilon_\perp$), and ϵ_0 is the permittivity of free space. For Eq. (1) to hold, the liquid crystal must be well into the temperature regime of the nematic phase where the magnitude of the order parameter is spatially constant and the elastic constants are only weakly temperature dependent. Some calculations have been done for the case where the electric field is zero [6–8] and for the radial-axial transition with weak perpendicular boundary conditions [9]. In general, however, a first-principle prediction of the director configurations, including prediction of the defect types and locations, is very difficult. Experiment therefore becomes the most realistic way to understand the behavior.

For submicron-sized nematic-liquid-crystal droplets, deuterium nuclear magnetic resonance has been used to determine the director configurations [10,11], whereas for supramicron-sized droplets, polarized optical microscopy is easier and more useful [2,12,13]. From pictures of droplets between crossed polarizers, droplets with bipolar, radial, and axial director configurations have been identified. A concentric director configuration has also been predicted and observed [12,14].

In reality, however, droplets may have structures more complicated than these basic configurations. Without an intensive analysis of the polarized droplet pictures, it is

often impossible to separate the more complicated configurations from the basic ones. For example, similar spiral textures of nematic-liquid-crystal droplets with perpendicular boundary conditions have been reported with alternate explanations [3,15]; and in the case of parallel surface anchoring, different microscopic textures have been claimed by different authors for similar appearing bipolar droplets [12,16].

In order to resolve these differences and to improve the quantitative identification of new types of droplet textures, computer simulated transmission patterns have been calculated for various model director structures [3,12]. A comparison of these calculated patterns with experimentally obtained patterns has proved to be a sensitive way of elucidating and refining the director structure. In particular, it is necessary to observe the drop using different polarizer orientations and with the electric field both parallel and perpendicular to the viewing direction. If all observations can then be simultaneously simulated using the same director model, one can be confident that the model is correct.

This procedure may be illustrated by showing results for the bipolar and concentric director configurations. Let the director be described by polar angle β and azimuthal angle γ as shown in Fig. 1:

$$\mathbf{n}=(n_x,n_y,n_z)=(\sin\beta\cos\gamma,\sin\beta\sin\gamma,\cos\beta)\ , \tag{2}$$

where β and γ are functions of the director position, expressed in spherical polar coordinates (r,θ,ϕ) or, alternatively, cylindrical coordinates (ρ,ϕ,z). The radius of the drop is **R**; an x-y cross section has radius $\rho_0(z)$. For the bipolar (subscript b) configuration [Fig. 2(a)], we use the model function

$$\beta_b=\left|\theta-\frac{\pi}{2}\right|\frac{\rho}{\rho_0}\ ,\quad \gamma_b=\phi\ , \tag{3}$$

and for the concentric (subscript c) configuration [Fig. 2(d)], we use the model function

$$\beta_c=\frac{\pi}{2}\ ,\quad \gamma_c=\phi+\frac{\pi}{2}\ . \tag{4}$$

We emphasize that (3) and (4) are not the result of free energy calculations, but rather functions which reproduce the essential features of the bipolar and concentric structures. Director configurations based on free energy minimization [8] produce transmission patterns qualitatively similar to those derived from Eqs. (3) and (4).

Putting these results in our droplet simulation program along with representative values for the refractive indices ($n_e=1.6$ and $n_0=1.5$), we obtain the calculated transmission patterns, between crossed polars, shown in Fig. 2. Figure 2(a) gives the bipolar director structure; note the appearance of two surface defects (boojums) at the poles. Figure 2(b) shows the transmission pattern of a bipolar drop with its axis aligned along the polarizer axis; Fig. 2(c) shows the same drop rotated between the polars by 22.5°. Figures 2(d)–2(f) show the same results for a concentric drop; here the defect is along a diameter containing the poles. Note that the two polarizer orientations give dramatically different pictures of the same drop. Also note that the signatures of the bipolar and

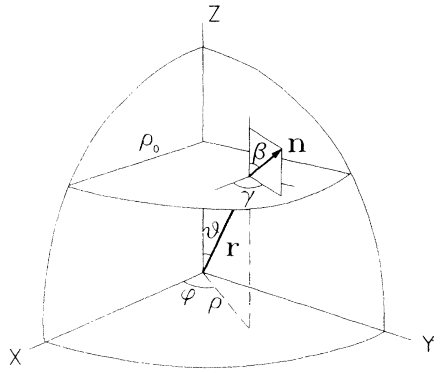

FIG. 1. Coordinates for describing director fields.

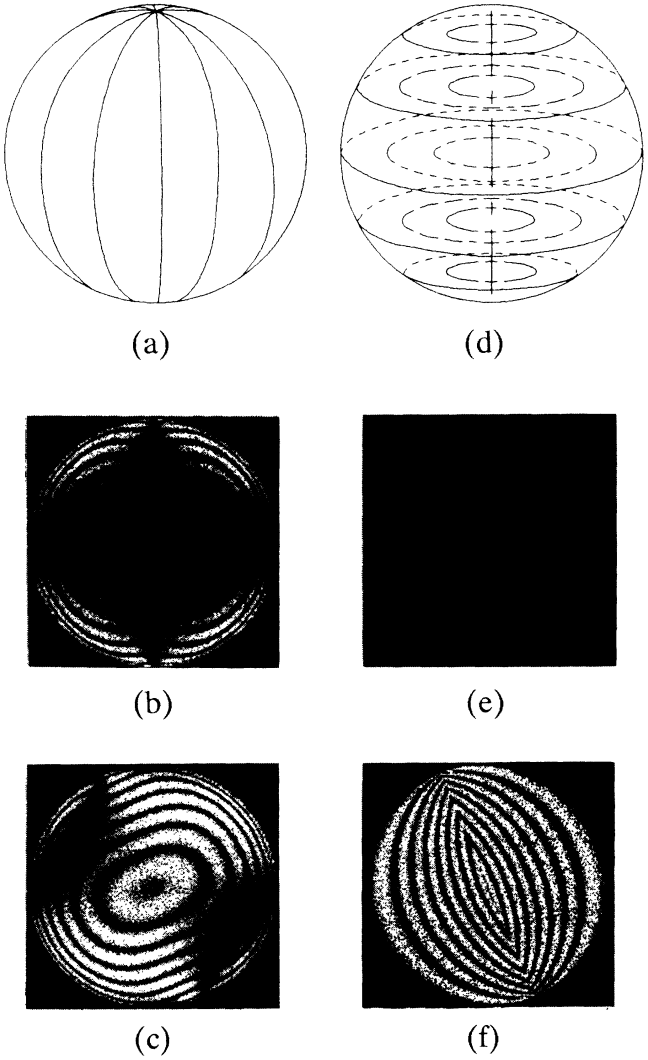

FIG. 2. Bipolar director field; (b) simulated transmission pattern of bipolar drop with radius = 24 μm, crossed polarizers parallel to axis (vertical in picture); (c) same as (b) but axis at 22.5° to polarizer; (d)–(f) same as (a)–(c) for a concentric drop.

concentric structures are themselves quite different, allowing one to readily distinguish between them.

We report here measurements by polarization microscopy of nematic-liquid-crystal droplets with negative dielectric anisotropy and parallel boundary conditions. Droplets were observed in electric fields either parallel or perpendicular to the observation direction and at different polarizer orientations. The director configuration of a droplet and the way it responds to the electric field have been determined by comparing the microscope pictures with computer-simulated transmission patterns from various models.

The algorithm of the computer simulations in this paper has been described previously [3,12]. Without the electric field, the director configuration of our droplets is described by combining features of both the bipolar and concentric configurations. This "twisted bipolar" structure has been described previously for spheres [7,16]; it is analogous to the "escaped twisted" structure found in cylinders with tangential boundary conditions by Cladis and Kleman [17]. When the electric field is turned on the droplet proves to be stable with its axis either perpendicular or parallel to the field. With increasing field, the structure becomes either more bipolarlike (axis initially perpendicular to the field) or more concentriclike (axis initially parallel to the field). At very high fields the bipolarlike texture evolves into a structure we call "escaped planar bipolar," which is analogous to the nonescaped planar bipolar structure found in cylinders by Ondris-Crawford *et al.* [18]. The concentric structure, on the other hand, is unstable in high fields, and through an unusual evolution of its defects, changes irreversibly into the escaped planar bipolar texture. The transition is in some respects analogous to the transition between the escaped planar and planar bipolar structures in cylinders described by Ondris-Crawford *et al.* [18], except in our case it is driven by an applied field rather than changes in surface anchoring energies or elastic constants.

II. EXPERIMENT

The matrix material employed in this experiment was composed of polyethylene glycol and polyvinyl pyrrolidone (Aldrich) and the liquid crystal was EN-18 (Chisso, Japan). Polyethylene glycol, a liquid polymer, imposes a parallel anchoring to EN-18, but due to the polymer's high density and low viscosity, the liquid crystal rapidly floats out of suspension and the droplets coalesce. To increase the matrix viscosity, polyvinyl pyrrolidone was dissolved into polyethylene glycol at 160 °C in a ratio of 49:51 by weight. The liquid crystal was then dispersed into the matrix by gentle stirring at 160 °C and the mixture was then quickly cooled to room temperature. The droplets were thus held in the matrix by its high room temperature viscosity.

For observation of droplets in electric fields applied parallel to the observation direction, the mixture was sandwiched between glass slides coated with transparent indium tin oxide. For observation in electric fields applied perpendicular to the observation direction, two parallel brass plates were placed between microscope slides to serve as both electrodes and spacers. The thickness of the plates was 500 μm; the spacing between them was 150 μm. 1-kHz ac electric fields were used in all measurements; reported voltages are rms values. All the photographs were taken with a Zeiss Universal microscope using a sodium lamp as the light source.

III. RESULTS AND COMPUTER SIMULATIONS

A. Zero electric field

Figure 3 shows the appearance of a droplet briefly exposed to a field lying in the plane of the picture but since removed. By comparing Fig. 3(a) to Fig. 2(f), one might conclude that it has a concentric structure. However, unlike Fig. 2(f) the axis of Fig. 3(a) is parallel to a polarizer, for which the concentric structure predicts complete darkness rather than the bright stripes seen. We therefore reject both the simple bipolar and concentric models. As a trial we construct a *twisted bipolar* director configuration composed of both bipolar and concentric configurations:

$$\mathbf{n}_{tb} = \sin(\alpha)\mathbf{n}_b + \cos(\alpha)\mathbf{n}_c \ , \tag{5}$$

where $\mathbf{n}_b$, $\mathbf{n}_c$, and $\mathbf{n}_{tb}$ are bipolar, concentric, and twisted bipolar directors, respectively, and α is the angle between the concentric and twisted bipolar directors [Fig. 4(a)].

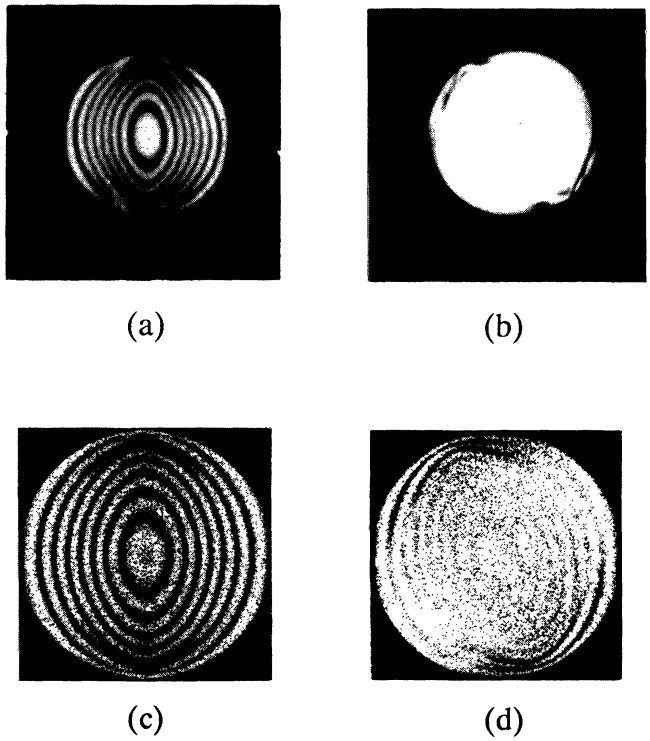

FIG. 3. (a) Photo of nematic-liquid-crystal droplet in zero field, radius $R = 24$ μm, between crossed polars with droplet axis parallel to polarizer (both vertical). (b) Same as (a) with axis at 22.5° to polarizer. (c),(d) Simulations corresponding to (a),(b) using the twisted bipolar model.

The concentric configuration has a line defect along the axis which is caused by $\alpha \neq 90°$. No such line defect was observed, however, and we therefore assume $\alpha \rightarrow 90°$ as $\rho \rightarrow 0$. That is, the twisted bipolar structure becomes purely bipolar near the axis. Our model for the director configuration is

$$\alpha = \frac{\pi}{2}[(1-\delta)e^{-\rho/\rho_0\xi_1} + \delta e^{-\rho/\rho_0\xi_2}] , \quad (6)$$

where ρ and ρ_0 are shown in Fig. 1. ξ_1 and ξ_2 are annealing lengths which give the distance from the axis over which the bipolar structure changes into the twisted bipolar structure. Although three parameters were required to most accurately simulate the observed transmission patterns, the contribution from ξ_2 is small due to the smallness of the admixture coefficient δ. Since these functions are those required to fit the data and not solutions to a free energy minimization, not too much significance should be attached to ξ_2.

Letting $\xi_1 = 0.8$, $\xi_2 = 2$, and $\delta = 0.05$, we get the director configuration shown in Fig. 4(b). The simulated transmission patterns from this model are compared with the experimental patterns in Fig. 3. The good agreement between the experimental and model transmission patterns indicates that the twisted bipolar configuration is very close to the actual one.

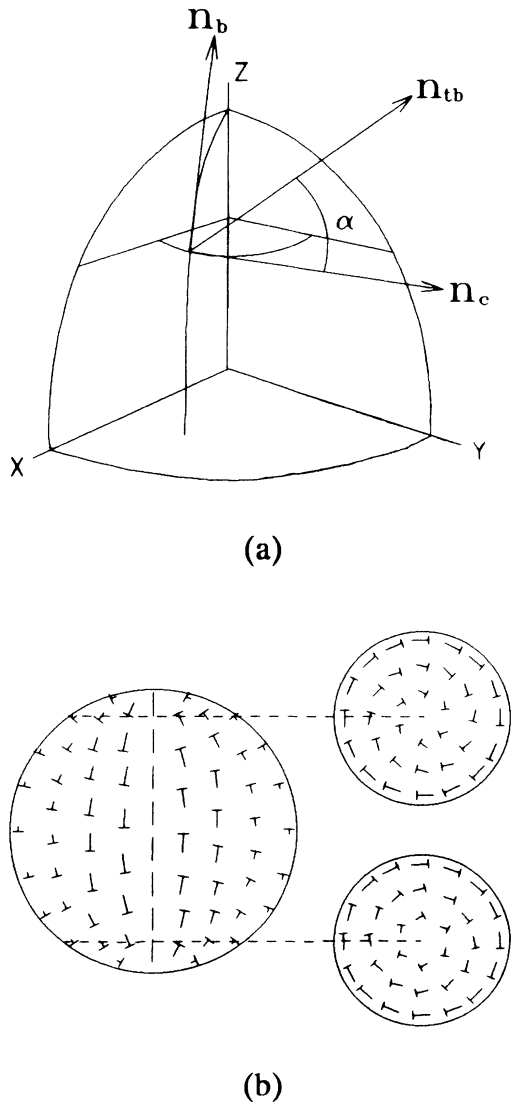

FIG. 4. (a) Parameters for describing the twisted bipolar model. See text for explanation of symbols. (b) Director field of twisted bipolar structure. Directors are shown as nails with lengths proportional to their projection on plane of page.

B. Axis perpendicular to the electric field

In a newly made sample the droplets are randomly oriented. Application of a weak electric field causes those droplets not initially closely aligned with the field to realign with their axes perpendicular to the field. Qualitatively, the bipolar component of the twisted bipolar structure should then increase as the field increases, since, due to the liquid crystal's negative dielectric anisotropy, the bipolar structure has more molecules aligned perpendicular to the field than the concentric structure.

This reasoning has been proved essentially correct if the electric field is not very high. Figure 5 shows experimental pictures of a droplet when the field is *parallel* to the light direction (perpendicular to the page). (a) and (b) show patterns for the polarizer at 0° and 22.5° to the droplet axis in a low field (38 kV/m); (c) and (d) are for the same polarizer angles but higher field (355 kV/m). Figure 6 shows the droplet when the field is *perpendicular* to the light direction. (a) and (b) are for polarizer angles of 0° and 45°, droplet axis perpendicular to the page, and high field (300 kV/m); (c) and (d) are the same drop at 700 kV/m, droplet axis tilted from the page normal, taken with and without polarizers.

Figures 5(a) and 5(b) look very similar to the simulated light transmission patterns shown in Figs. 2(b) and 2(c) for the bipolar model. Note, however, that the dark cross in Fig. 5(a) is not completely black, which, we attribute to a small amount of twist. At high fields, "strained" regions can been seen; these occur at the top and bottom of Fig. 5(c) and in Fig. 6(d). By analyzing the photographs we conclude that the strained region is a ring containing the field direction in its plane. We explain this ring by proposing the *escaped planar bipolar* model, which is constructed in the following way.

Let the electric field be oriented in the z direction and the bipolar boojums lie on the x axis. We first construct a *planar bipolar* structure [Fig. 7(a)] in which all the directors are perpendicular to the z direction and in each plane perpendicular to the z direction a planar bipolar structure is formed. The poles lie on the great circle given by $x^2+z^2=R^2$ and $y=0$. The escaped planar bipolar model is obtained by escaping the poles of the 2D bipolar sheets along the circle to the two boojums, shown in Fig. 7(b). We should point out that Bezić and Žumer have proposed an escaped planar bipolar structure for chiral nematics in infinite cylinders [19]. In their structure, however, the escaped lines spiral about the cylinder surface and, unlike our structure, no boojums are involved.

A mathematical description of the escaped planar bi-

polar structure is given by

$$\mathbf{n}_{epb}=\frac{w_{tb}\mathbf{n}_{tb}+w_{pb}\mathbf{n}_{pb}}{|w_{tb}\mathbf{n}_{tb}+w_{pb}\mathbf{n}_{pb}|}\ , \tag{7}$$

where $\mathbf{n}_{tb}$ and $\mathbf{n}_{pb}$ are the directors of the twisted bipolar [Eq. (6)] and planar bipolar [Eq. (3)] structures, respectively, and w_{tb} and w_{pb} are their weights in the combination. At high fields, ξ_1 and ξ_2 in the twisted bipolar model should be much larger than the radius of the droplet, so the twisting is practically negligible. The bipolar director configuration dominates only around the ring

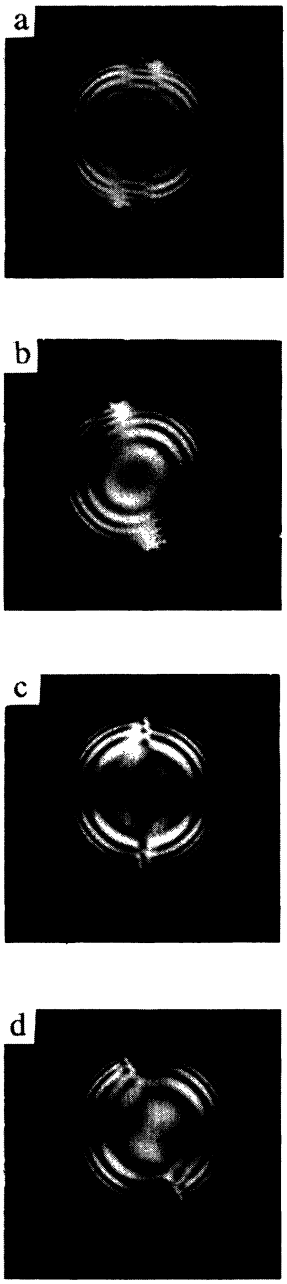

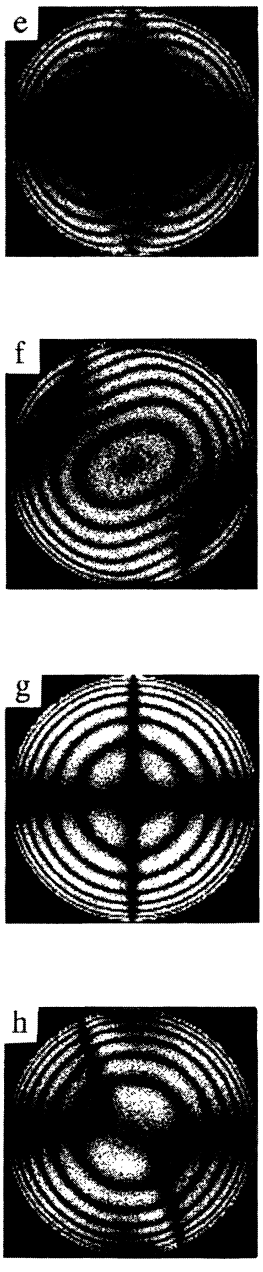

FIG. 5. Experimental [(a)–(d)] and simulated [(e)–(h)] transmission patterns of twisted bipolar droplets with the droplet axis in the plane of the figure, and **E** perpendicular to the droplet axis and parallel to the light. (a)–(b) Axis at 0° and 22.5° to the polarizer (vertical in the plane of figure), $E=38$ kV/m; (c),(d) same as (a) and (b), but $E=355$ kV/m; (e)–(h) are simulations of (a)–(d) using twisted bipolar model with $\delta=0.05$, $\xi_1=0.8$, and $\xi_2=2$.

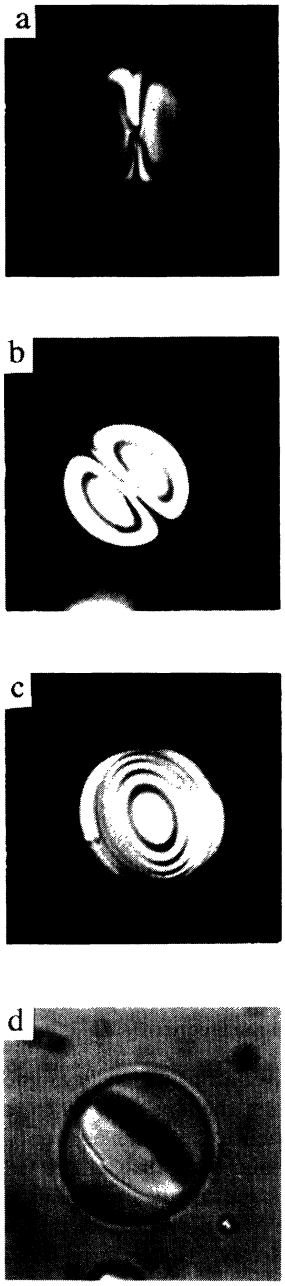

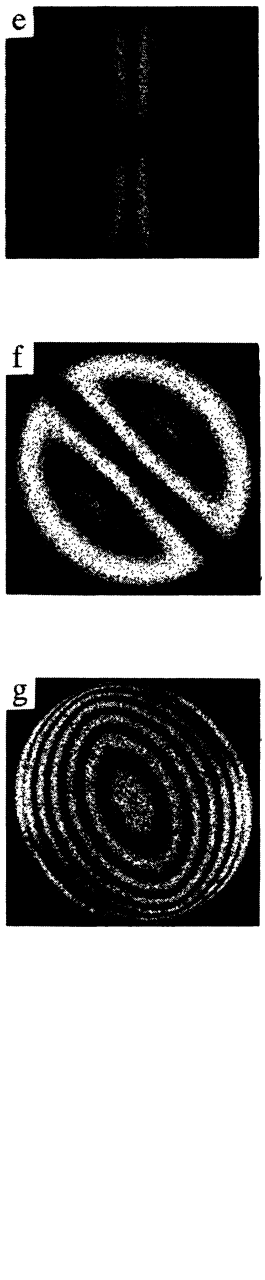

FIG. 6. Experimental [(a)–(d)] and simulated [(e)–(g)] transmission patterns of twisted bipolar droplets with axis in the plane of the paper, and **E** perpendicular to droplet axis and perpendicular to light. (a)–(b) Axis perpendicular to paper; **E**=300 kV/m at 0° and 45° to polarizer axis (vertical in the plane of the figure). (c),(d) Same drop at 700 kV/m, axis tilted away from page normal, with and without polarizers. (e),(g) are simulations of (a)–(c) using twisted bipolar model.

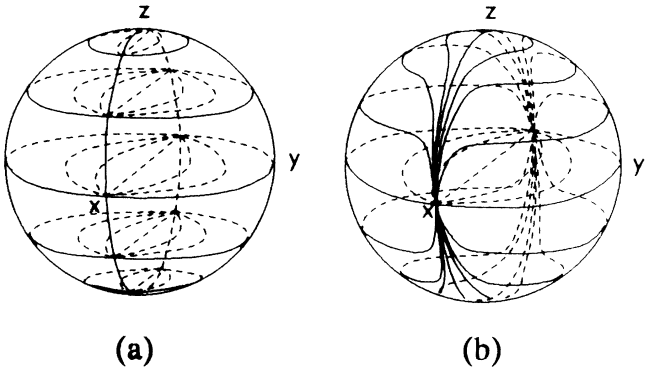

FIG. 7. (a) The planar bipolar model; (b) the escaped planar bipolar model.

($R-r=0$ and $|y|=0$), so we take the weights to be

$$w_{tb}=e^{-[|y|+(R-r)]/\eta}\ ,$$
$$w_{pb}=\sqrt{1-w_{tb}^2}\ , \tag{8}$$

where η is roughly the width of the escaped region.

The simulations from this model are given in Figs. 5(e)–5(h) and Figs. 6(e)–6(g). In Figs. 5(e)–5(f), the electric field is large enough to remove the twist from the twisted bipolar structure but not large enough to distort it to the escaped planar bipolar. The structure is therefore essentially bipolar, which we model by taking $\eta=10^3R$ (negligible escape) and $\xi_1=10$ (very little twist). A comparison to experiment [Figs. 5(a)–5(b)] shows good agreement.

For Figs. 5(g)–5(h) and Figs. 6(e)–6(g), the field is large enough to remove the twist and transform the droplet into the escaped planar bipolar structure. We model this structure by choosing $\eta=0.1R$ (extensive escape) and $\xi_1=1000$ (negligible twist). Again, comparison with the experiment pictures is good. Since the experimental pictures and simulations are views of the same drop in many different ways, we feel that the escaped planar bipolar model is the correct one.

C. Initial axis parallel to the electric field

For those drops whose axes are initially closely aligned with the electric field, a rotation of the axis *parallel* to the field takes place. One might then expect the concentric structure to win against the bipolar structure as the field increases, since the concentric structure has all its molecules lying perpendicular to the field direction, as desired by the negative dielectric anisotropy. However, a purely concentric director configuration has a line defect along its axis of symmetry which is energetically unfavorable; as a result the bipolar-like escape along the droplet axis still survives. We call this structure *escaped concentric.*

Figure 8 shows microscope photographs of a droplet with its axis parallel to the electric field (both in the plane of the picture), taken at two field strengths. In Fig. 8(a) the field is relatively small (21 kV/m) and the axis and field are aligned with the polarizers. In Figs. 8(b)–8(d) the field is increased to 131 kV/m and the droplet is pictured with the microscope stage rotated at 0°, 9°, and 22.5°. The structure corresponding to these pictures is the escaped concentric. Here an increasing field causes the outer regions of the droplet to become more concentric while the radius of the central twisted bipolar region becomes narrower.

These features can be accounted for in the simulation

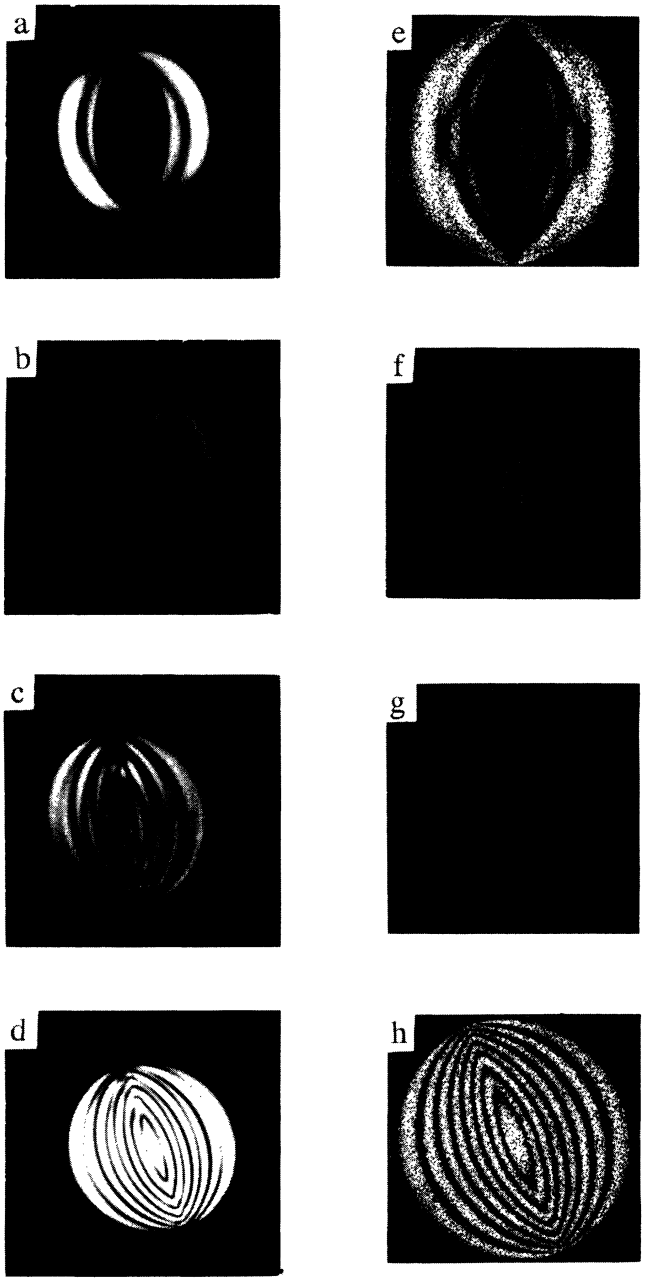

FIG. 8. Experimental [(a)–(d)] and simulated [(e)–(h)] transmission patterns for **E** parallel to droplet axis and perpendicular to light. (a) $E=21$ kV/m at 0° to polarizer; (b)–(d) $E=131$ kV/m at 0°, 9°, and 22.5° to polarizer; (e)–(h) simulations of (a)–(d) using twisted bipolar model, which $\xi_1=0.4$, $\xi_2=2$, and $\delta=0.05$ for (e); $\xi_1=0.05$, $\xi_2=2$, $\delta=0.03$ for (f)–(h), and $\eta=10^4R$ for all.

by using Eqs. (7) and (8) and taking $\eta=10^4R$, which yields the twisted bipolar model of Eqs. (5) and (6). For droplets with their axes parallel to the electric field and the polarizer [Figs. 8(a)–8(b)], a dark core is exhibited which becomes smaller as the field increases. This feature is well simulated by the twisted bipolar model. Also, droplets in high fields with their axes at a slight angle to the polarizer [Fig. 8(c)] exhibit stripes of alternating brightness. This feature could not be simulated if a single exponential function were used in Eq. (3), but good agreement could be achieved by adding the second exponential term with $\delta=0.03$ and $\xi_2=2$ in Eq. (6) [see Figs. 8(c) and 8(g)]. Again, too much significance should not be attached to this extra term, since it does not change the topology of the director configuration and hardly changes the actual director angles.

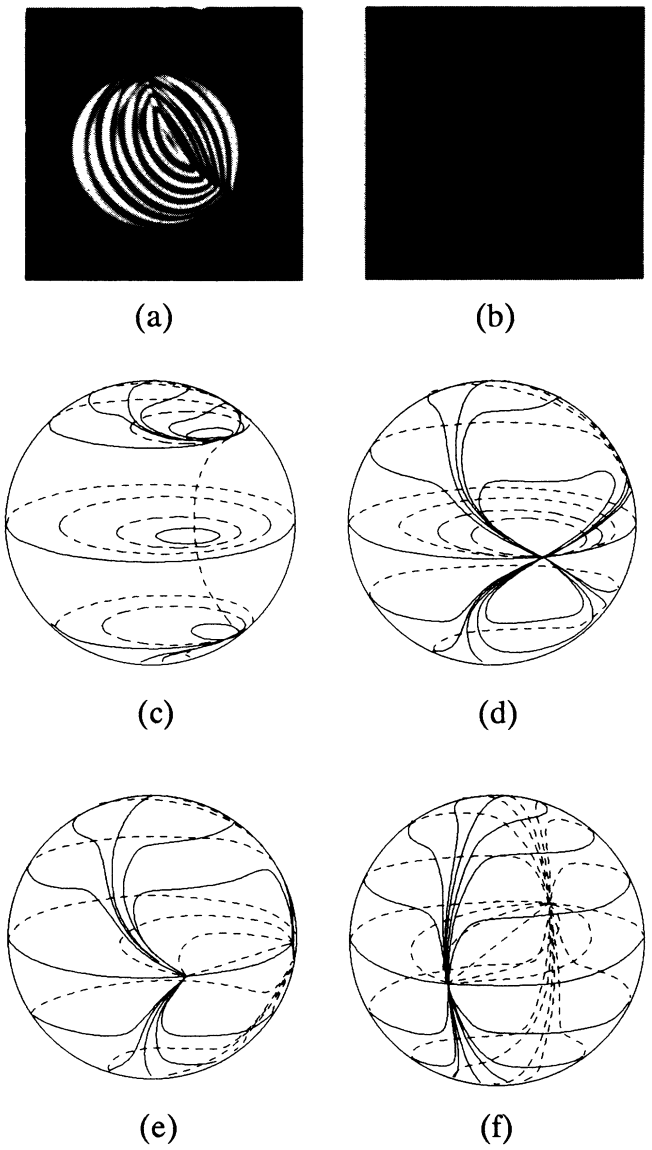

FIG. 9. (a),(b) Microscope photographs of instability in drops with axis parallel to E and $E=667$ kV/m. (c)–(f) Explanation of instability transition from concentric to escaped planar bipolar structure. (c) $s=+1$ concentric boojums move toward each other causing escaped line to bend; (d) boojums combine to form single $s=+2$ boojum; (e) $s=+2$ boojum splits into two radial $s=+1$ boojums; (f) $s=+1$ boojums migrate to diametrically opposite positions to form escaped planar bipolar structure.

D. Transition from concentric to escaped planar bipolar

When droplets with their axes parallel to the field are subjected to sufficiently high fields, the escaped concentric structure becomes unstable and the droplet reverts to the escaped planar bipolar structure previously described for droplets with their axes perpendicular to the field. The transition is not chaotic, however, but takes place over a time of a few seconds via distinct, but unstable, intermediate states. Although we have not done any specific calculations for this transition, Fig. 9 offers a speculative explanation for the evolution of the transition.

The first evidence of the transition is a spontaneous bending of the escaped line in the escaped concentric structure as shown in Fig. 9(a). The two surface defects, described as $s=+1$ *concentric* defects in a two dimensional director picture, begin to move together [Fig. 9(b)] and new "strain lines" can be seen. Figures 9(c)–9(f) are diagrams showing the subsequent development, which was seen visually but took place too rapidly to be photographed. Figure 9(c) shows the curved central region; also, it offers an explanation of the strain lines seen in Fig. 9(b). In Fig. 9(d) the line has shrunk to a point and the two surface defects have combined to form a single $s=+2$ surface defect. This defect is also unstable, however, and it splits into two $s=+1$ *radial* surface defects [Fig. 9(e)]. These defects then migrate to opposite ends of a diameter perpendicular to the field and the drop takes the escaped planar bipolar structure [Fig. 9(f)].

We point out that this transition is irreversible. If the field is reduced to zero the drop does not return to the concentric structure, but rather returns to the twisted bipolar structure with the axis remaining perpendicular to the field.

IV. CONCLUSIONS

We have combined polarized microscopy of nematic-liquid-crystal droplets with computer simulated, model-dependent transmission patterns in order to elucidate the director structure in the presence of electric fields. While the observed droplet transmission patterns have features common to previously reported bipolar and concentric configurations, detailed examination reveals that the director configurations are more complex.

In the zero-field state, the structure is twisted bipolar, evolving into either more bipolar-like or concentric-like structures as the field increases. At high fields, the concentric-like structure is unstable and transforms irreversibly to the twisted bipolar structure.

It should now be possible to compare the spatial behavior of the director reported here with that derived from a minimization of the free energy. In particular, it should be possible to determine how the addition of twist

minimizes the free energy at zero field, and what the conditions of stability are for a zero-field droplet at various orientations in a weak electric field. As the field increases, calculations should be able to show the evolution of the director configuration from the twisted bipolar to escaped planar bipolar structures and the instability of the concentric structure at high fields. These calculations are currently being investigated.

ACKNOWLEDGMENTS

We would like to thank P. Collings for useful discussions. H.-S. K. acknowledges financial support from the Deutsche Forschungsgemeinschaft (Sfb 335); F. X. and P. P. C. are supported by the Office of Technology Transfer and Economic Development, University of Hawaii.

[1] J. W. Doane, in *Liquid Crystals: Applications and Uses,* edited by B. Bahadur (World Scientific, Singapore, 1990), Vol. 1, Chap. 14; H.-S. Kitzerow, Liq. Cryst. **16**, 1 (1994).

[2] V. G. Bondar, O. D. Lavrentovich, and V. M. Pergamenshchik, Zh. Eksp. Teor, Fiz **101**, 111 (1992) [Sov. Phys. JETP **74**, 60 (1992)]; D. K. Yang and P. P. Crooker, Liq. Cryst. **9**, 245 (1991).

[3] F. Xu, H.-S. Kitzerow, and P. P. Crooker, Phys. Rev. A **46**, 6535 (1992).

[4] J. H. Erdmann, S. Žumer, and J. W. Doane, Phys. Rev. Lett. **64**, 1907 (1990).

[5] See, for example, P. W. Anderson, *Basic Notions of Condensed Matter Physics* (Benjamin, Menlo Park, CA, 1984), p. 58 and references therein.

[6] M. J. Press and A. S. Arrot, Phys. Rev. Lett. **33**, 403 (1974).

[7] R. D. Williams, J. Phys. A **19**, 3211 (1986).

[8] E. Dubois-Violette and O. Parodi, J. Phys. (Paris) Colloq. **30**, C4-57 (1969).

[9] S. Kralj and S. Žumer, Phys. Rev. A **45**, 2461 (1992).

[10] A. Golemme, S. Žumer, J. W. Doane, and M. E. Neubert, Phys. Rev. A **37**, 559 (1988).

[11] A. Golemme, S. Žumer, D. W. Allender, and J. W. Doane, Phys. Rev. Lett. **61**, 2937 (1988).

[12] R. Ondris-Crawford, E. P. Boyko, B. G. Wagner, J. H. Erdmann, S. Žumer, and J. W. Doane, J. Appl. Phys. **69**, 6380 (1991).

[13] P. S. Drzaic, J. Appl. Phys. **60**, 2124 (1986).

[14] P. S. Drzaic, Mol. Cryst. Liq. Cryst. **154**, 289 (1988).

[15] O. D. Lavrentovich and E. M. Tarent'ev, Zh. Eksp. Teor. Fiz. **91**, 2084 (1986) [Sov. Phys. JETP **64**, 1237 (1986)].

[16] A. V. Koval'chuk, M. V. Kurik, O. D. Lavrentovich, and V. V. Sergan, Zh. Eksp. Teor. Fiz **94**, 350 (1988) [Sov. Phys. JETP **67**, 1065 (1988)].

[17] P. E. Cladis and M. Kleman, J. Phys. **33**, 591 (1972).

[18] R. J. Ondris-Crawford, G. P. Crawford, S. Žumer, and J. W. Doane, Phys. Rev. Lett. **70**, 194 (1993).

[19] J. Bezić and S. Žumer, Liq. Cryst. **14**, 1695 (1993); see Fig. 6(b) for their escaped planar bipolar structure.

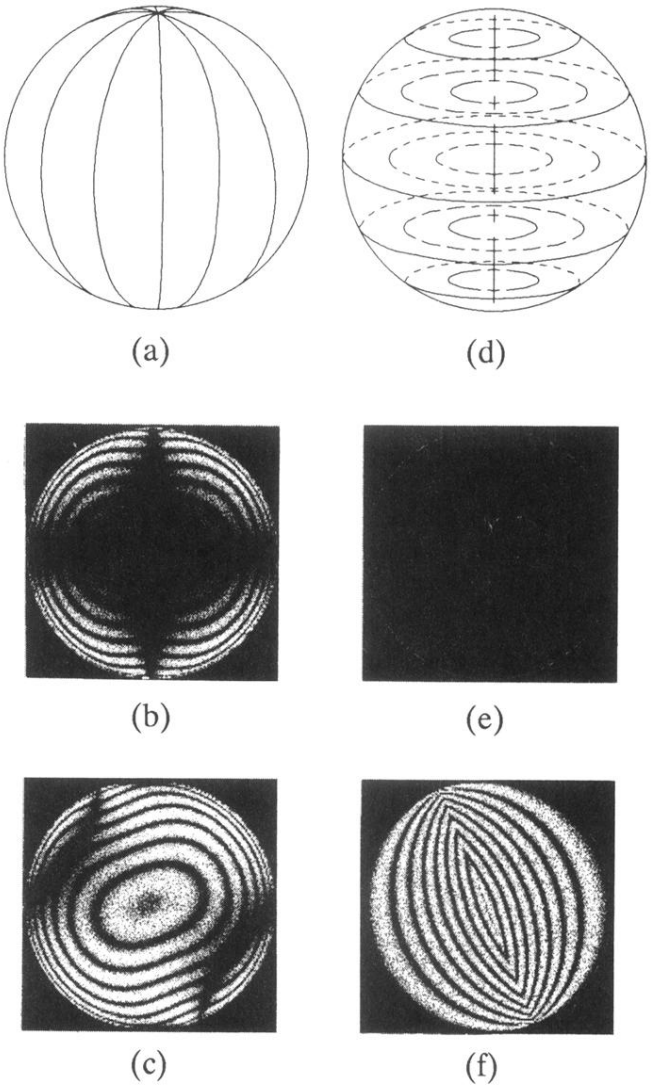

FIG. 2. Bipolar director field; (b) simulated transmission pattern of bipolar drop with radius = 24 μm, crossed polarizers parallel to axis (vertical in picture); (c) same as (b) but axis at 22.5° to polarizer; (d)–(f) same as (a)–(c) for a concentric drop.

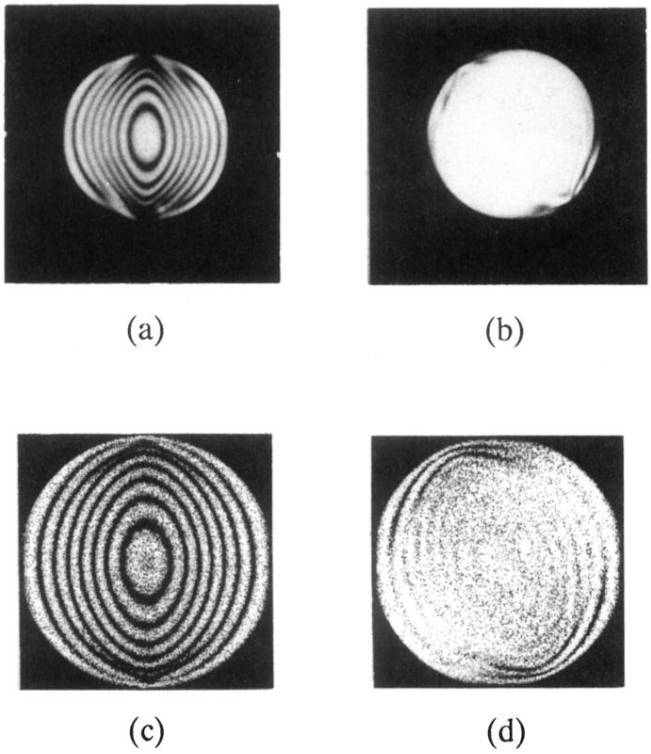

FIG. 3. (a) Photo of nematic-liquid-crystal droplet in zero field, radius $R = 24$ μm, between crossed polars with droplet axis parallel to polarizer (both vertical). (b) Same as (a) with axis at 22.5° to polarizer. (c),(d) Simulations corresponding to (a),(b) using the twisted bipolar model.

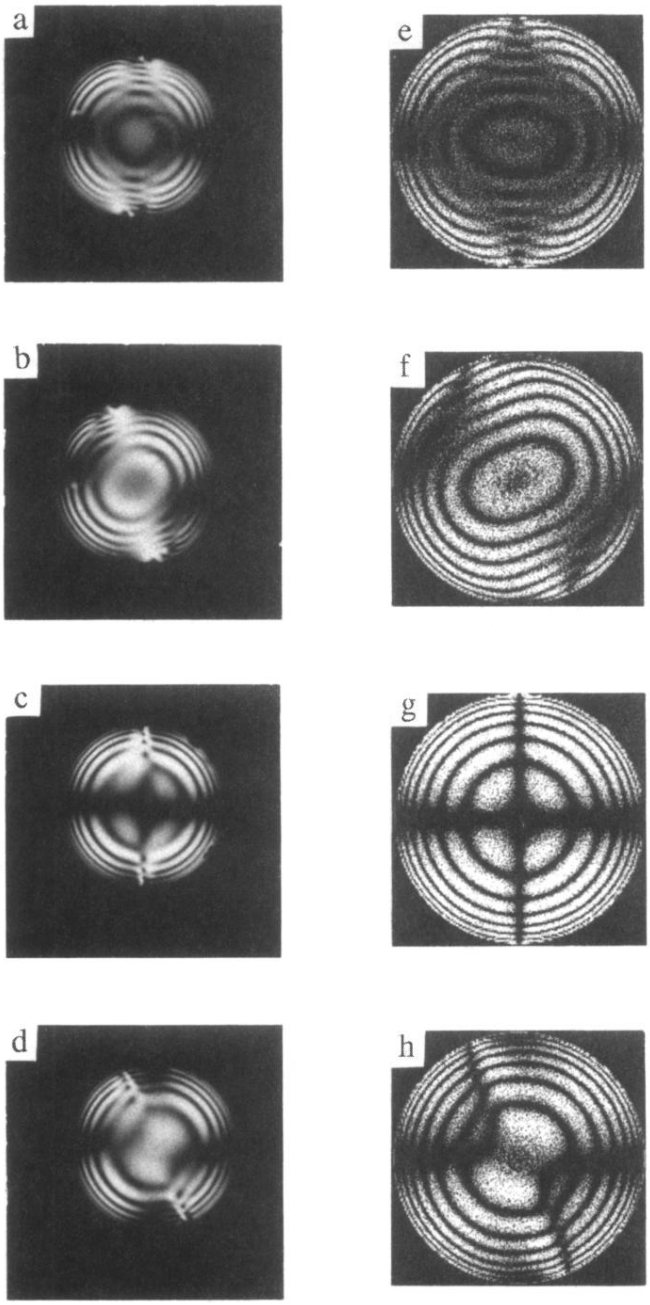

FIG. 5. Experimental [(a)–(d)] and simulated [(e)–(h)] transmission patterns of twisted bipolar droplets with the droplet axis in the plane of the figure, and **E** perpendicular to the droplet axis and parallel to the light. (a)–(b) Axis at 0° and 22.5° to the polarizer (vertical in the plane of figure), $E=38$ kV/m; (c),(d) same as (a) and (b), but $E=355$ kV/m; (e)–(h) are simulations of (a)–(d) using twisted bipolar model with $\delta=0.05$, $\xi_1=0.8$, and $\xi_2=2$.

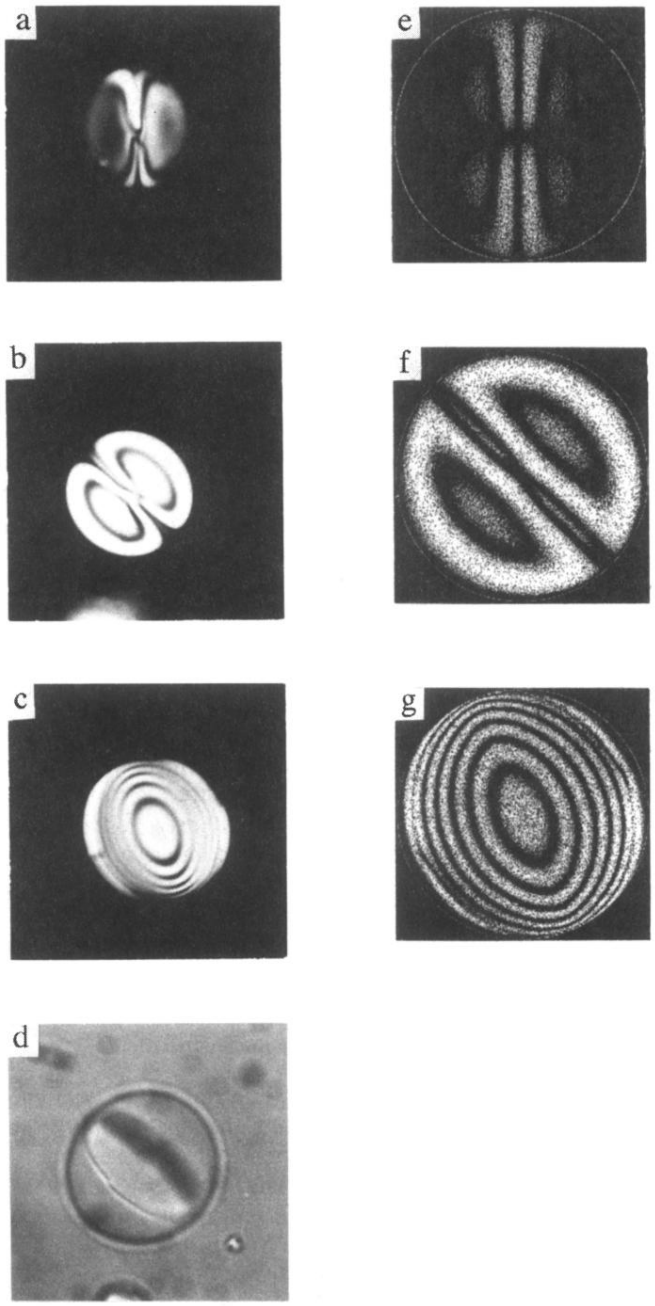

FIG. 6. Experimental [(a)–(d)] and simulated [(e)–(g)] transmission patterns of twisted bipolar droplets with axis in the plane of the paper, and **E** perpendicular to droplet axis and perpendicular to light. (a)–(b) Axis perpendicular to paper; $\mathbf{E}=300$ kV/m at 0° and 45° to polarizer axis (vertical in the plane of the figure). (c),(d) Same drop at 700 kV/m, axis tilted away from page normal, with and without polarizers. (e),(g) are simulations of (a)–(c) using twisted bipolar model.

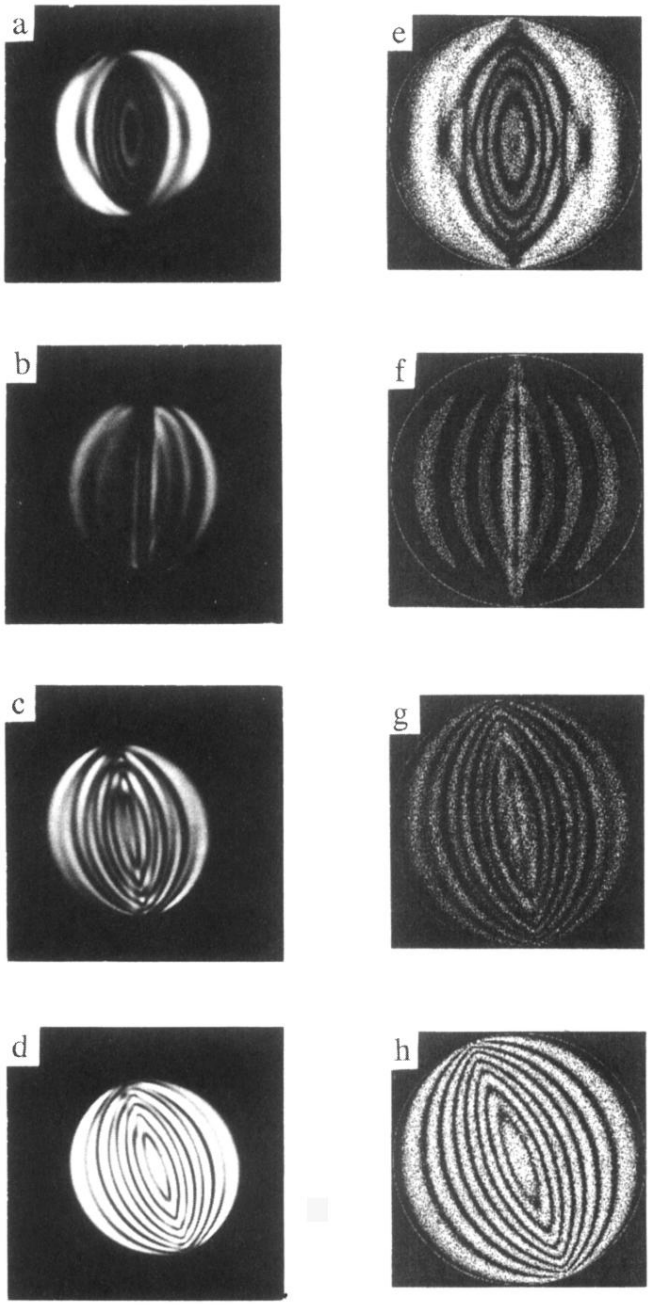

FIG. 8. Experimental [(a)–(d)] and simulated [(e)–(h)] transmission patterns for **E** parallel to droplet axis and perpendicular to light. (a) $E=21$ kV/m at 0° to polarizer; (b)–(d) $E=131$ kV/m at 0°, 9°, and 22.5° to polarizer; (e)–(h) simulations of (a)–(d) using twisted bipolar model, which $\xi_1=0.4$, $\xi_2=2$, and $\delta=0.05$ for (e); $\xi_1=0.05$, $\xi_2=2$, $\delta=0.03$ for (f)–(h), and $\eta=10^4R$ for all.